Physically Realizing an Optimized Sparse Spectrum via Joint Design of a Collection of FM Waveforms

Peng Seng Tan[1,2], James M. Stiles[2], Shannon D. Blunt[2]
[1]Innovation Group, Eaton Lighting Division, Peachtree City, Georgia
[2]Radar Systems Lab (RSL), University of Kansas, Lawrence, KS

***Abstract*—Within a Marginal Fisher's Information (MFI) framework, the design of disjoint coherent frequency allocations is examined for the purpose of spectrum sharing. While the overall bandwidth establishes the radar range resolution, it is possible to reallocate a portion of this bandwidth to other users for a trade-off in terms of increased range sidelobes. For a given percent allocation for radar usage, MFI is used to search for advantageous disjoint frequency distributions from the standpoint of minimizing sidelobe degradation, along with an imperative to maintain spectral cohesion to the degree possible (i.e. keep the number of contiguous bands to a minimum). It is then demonstrated that individual polyphase-coded FM (PCFM) waveforms can be associated with these bands to optimize the collective radar emission jointly.**

Keywords—spectrum sharing, Cramer-Rao bound, waveform optimization

I. INTRODUCTION

With the introduction of cellular 5G technology [1], as well as new Wi-Fi protocols such as 802.11ac for the Internet-of-Things [2] and IEEE 802.11p for vehicular communication [3], challenges to radar spectral primacy are rapidly increasing [4]. In response to these challenges new spectrum-sharing capabilities are likewise emerging at an increasing rate (e.g. [5-30]).

Particularly relevant here is the placement of notches in the radar transmit spectrum to avoid interfering with other spectrum users (see [5-10, 17, 20, 21-23]). Specifically, we expand on the work in [19] where, for a given percent allowable spectral occupancy, optimization according to marginal Fisher's Information (MFI) [31-34] was used to determine the allocation of sub-bands such that the resulting trade-off in terms of increased radar range sidelobes is minimized. This manner of spectral thinning is analogous to the minimum redundancy concept for sparse antenna array design [35].

Here we extend this theoretical formulation by forcing the allocation optimization to adhere to minimum-width spectral blocks denoted as "meso-bands" (MBs), each comprised of a collection of sub-bands, as a means to facilitate reduced spectral fragmentation. The combination of these MBs adheres to the specified percent allocation of the total bandwidth while still providing a range resolution, when pulse compressed collectively, that is the same as what would be achieved for use of the total bandwidth. A similar notion of meso-band formation was explored in [36], albeit for the purpose of fast spectrum sensing (and usage of the terms sub-band and meso-band is different here).

For each MB resulting from the allocation optimization, an FM waveform is then generated, with the ultimate physical sparse-spectrum radar emission being the superposition of this collection of waveforms. It is shown that this emission can easily be produced by a set of disjoint LFM waveforms having the MFI-prescribed MBs and relative frequency offsets. It is also shown that the overall sparse-spectrum emission can be optimized via different parameterized versions of the individual FM waveforms [37-39].

II. RADAR MEASUREMENT MODEL AND MFI

Consider the set of L range domain scattering measurements described using the linear model

$$\mathbf{v} = \mathbf{H}\boldsymbol{\gamma} + \mathbf{n}\,, \tag{1}$$

with observation vector $\mathbf{v}$ represented in the frequency domain, the $M \times 1$ vector $\boldsymbol{\gamma}$ corresponding to the complex scattering as a function of range, the $L \times 1$ vector $\mathbf{n}$ containing additive noise, and the $L \times M$ observation matrix $\mathbf{H}$ relating the set of scatterers to the L measurements. Putting (1) in the sparse spectrum context, the bandwidth B is discretized into M sub-bands and we wish to determine the particular $L < M$ sub-bands that provide the best estimate of $\boldsymbol{\gamma}$. As posed in [20], the particular value of $M = B$ / PRF specifies the sampling of the line spectra, for PRF the pulse repetition frequency.

It was shown in [32] that an error covariance matrix can be defined for the measurement model in (1) as

$$\mathbf{K}_{\varepsilon} = E\{\boldsymbol{\varepsilon}\boldsymbol{\varepsilon}^{H}\}\,, \tag{2}$$

where $\boldsymbol{\varepsilon} = \boldsymbol{\gamma} - \hat{\boldsymbol{\gamma}}$ for estimate $\hat{\boldsymbol{\gamma}}$. From a radar pulse compression standpoint this error takes the form of range (and possibly Doppler) sidelobes. The Cramer-Rao lower bound (CRLB) of this estimate is the inverse of the Fisher information matrix

$$\mathbf{J} = E\left\{\left[\nabla_{\boldsymbol{\gamma}} \ln\left(f_{\mathbf{v}|\boldsymbol{\gamma}}(\mathbf{v})\right)\right]\left[\nabla_{\boldsymbol{\gamma}} \ln\left(f_{\mathbf{v}|\boldsymbol{\gamma}}(\mathbf{v})\right)\right]^{H}\right\}, \tag{3}$$

for $\nabla_{\boldsymbol{\gamma}}$ the gradient operator and $f_{\mathbf{v}|\boldsymbol{\gamma}}(\mathbf{v})$ the probability density of $\mathbf{v}$ given $\boldsymbol{\gamma}$ [40,41]. This bound is achieved when one applies the minimum mean-square error (MMSE) estimator of $\boldsymbol{\gamma}$ [32].

The notion of marginal Fisher's information (MFI) [31-34] was developed as a means to optimize the measurement operation and is related to the theory of optimal experiments [42]. Generally speaking, MFI measures the amount of new information that is obtained by adding a new ℓth measurement to a previous set of $(\ell-1)$ measurements, which can be stated in terms of (3) as

$$\text{MFI} = \frac{1}{M}\text{tr}\left\{\Delta\mathbf{K}_{\varepsilon}(\ell)\right\} \tag{4}$$

for

$$\begin{aligned}\Delta\mathbf{K}_{\varepsilon}(\ell) &= \mathbf{K}_{\varepsilon}(\ell) - \mathbf{K}_{\varepsilon}(\ell-1) \\ &= \mathbf{J}^{-1}(\ell) - \mathbf{J}^{-1}(\ell-1)\end{aligned}. \tag{5}$$

Here tr{•} is the trace operation, $\mathbf{J}^{-1}(\ell)$ is the inverse Fisher information matrix based on ℓ measurements, and use of the MMSE estimator is assumed.

In other words, for a given limit on percent spectral occupancy by the radar, Fisher's information establishes the metric $\text{tr}\{\mathbf{K}_{\varepsilon}\} = \text{tr}\{\mathbf{J}^{-1}\}$, the minimization of which determines the particular set of $L < M$ sub-bands within the overall bandwidth B that minimize error in the form of range sidelobes. The MFI metric of (4) is therefore a strategy to ascertain this set by establishing how much unique information each measurement provides.

In [20] the MFI approach summarized above was used to optimize the sparse allocation of $L < M$ sub-bands distributed over bandwidth B. However, in so doing the distribution of sub-bands tended to be rather fragmented, which does not actually achieve the intended goal of permitting allocations of in-band radar spectrum to other users and effectively hinders the formation of realistic radar waveforms. Here these attributes are addressed by forcing the sparse radar spectral content to adhere to meso-bands (contiguous blocks of sub-bands). As such, we can subsequently form physical radar waveforms for these meso-bands that collectively realize the radar emission, which can then be assessed relative to other physical radar emissions.

Where [20] allowed the L sub-bands to reside in any configuration among the M possible spectral locations, now P meso-bands are formed. Each meso-band consists of Q sub-bands such that the total $L = PQ$ is preserved and the percent spectral occupancy is still determined by L / M. Thus the spectral granularity (i.e. how large is M) is arbitrary as long as this ratio is maintained.

The MFI approach is applied to allocate these P meso-bands according the criterion in (4). The first stage involves the initial placement of the meso-bands, where the particular spectral location of each additional meso-band is selected according to the maximal reduction in error. While it would stand to reason that a condition that ensures new meso-bands do not overlap existing meso-bands should be enforced, such is actually not necessary because overlapping would penalize the amount of reduced error and thus is naturally avoided.

Once the P meso-bands have been assigned, (4) is again applied to determine whether there is a change in the location of any of the P meso-bands that would afford further error reduction. This process may be performed in the same order as the meso-band placement or could be randomized. This procedure is summarized in Table 1.

Simply put, the MFI approach is searching for any single meso-band change that provides improvement. Clearly this greedy approach is not guaranteed to find the optimum sparse allocation. More complicated "double-swap" or even "multi-swap" approaches could be used, though the computational cost would be considerably higher. Further, given the fact that a pulsed waveform cannot actually be perfect bandlimited, and by extension neither can the waveforms associated with the individual meso-band allocations, it is unclear whether the theoretically optimum sparse allocation would truly be so for a practical radar emission anyway (not to mention transmitter distortion effects [43]).

TABLE I. MFI-BASED SPARSE SPECTRUM ALLOCATION

1.	Assign the first meso-band at either of the edges of the total bandwidth B.
2.	For $p = 2, 3, \ldots, P$, allocate the pth meso-band to the particular set of Q contiguous sub-bands that minimize $\Delta\mathbf{K}_{\varepsilon}(p) = \mathbf{K}_{\varepsilon}(p) - \mathbf{K}_{\varepsilon}(p-1)$.
3.	With all P meso-band allocations completed, either sequentially or randomly select the pth meso-band and determine whether there exists a new assignment such that $\Delta\mathbf{K}_{\varepsilon} = \mathbf{K}_{\varepsilon,\text{new}} - \mathbf{K}_{\varepsilon,\text{current}}$ is negative. If so, reallocate the pth meso-band to this new assignment.
4.	Once no further single changes that provide an error reduction are possible, the MFI-optimized sparse spectrum allocation is obtained.

As an example, consider the case in which $M = 400$ and 50% of B is allocated for use by the radar (so $L = 200$). By applying MFI based only on sub-bands as in [20], the spectrum allocation in Fig. 1 was obtained, where a small blue dot signifies the assignment of a sub-band. While it might appear that far more than 50% of the spectrum has been assigned, what has actually occurred is that MFI has naturally dispersed the allocated sub-bands to maximally exploit the available spectrum of $M = 400$ sub-bands with the limited resource of $L = 200$ allowed sub-bands.

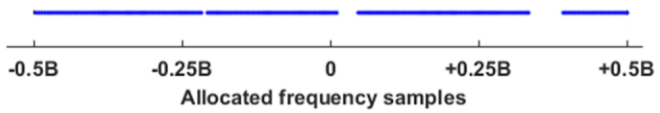

Figure 1. MFI-based sparse spectrum allocation for 50% usage of the total spectrum using sub-band assignment

In contrast, for the same $M = 400$ possible sub-bands and 50% radar allocation, now consider the use of $P = 40$ meso-bands, each comprised of $Q = 5$ sub-bands (so that we still have $40 \times 5 = 200 = L$). Now the MFI sparse-spectrum optimization of Table 1 realizes the allocation depicted in Fig. 2. It is immediately obvious that this spectrum allocation contains far more available spectral regions of practical utility for another user or users.

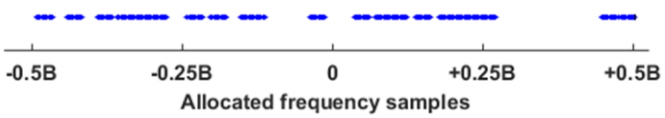

Figure 2. MFI-based sparse spectrum allocation for 50% usage of the total spectrum using meso-band assignment

To evaluate the goodness of these sparse spectral allocations from the perspective of providing usable available bandwidth, consider the fragmentation metric

$$\%B \text{ for which } B_{\text{contig}} \geq B_{\text{usable}}, \tag{6}$$

which determines the percent of overall bandwidth B that possesses a contiguous available bandwidth B_{contig} that meets or exceeds some minimum usable bandwidth B_{usable}. For the allocations in Figs. 1 and 2, this metric is plotted in Fig. 3 as a function of the usable bandwidth. For example, if B_{usable} is set to 2.5% of B, the allocation based on sub-bands (Fig. 1) only realizes 9.6% of the spectrum that meet this criterion while the meso-band allocation (Fig. 2) achieves 42%.

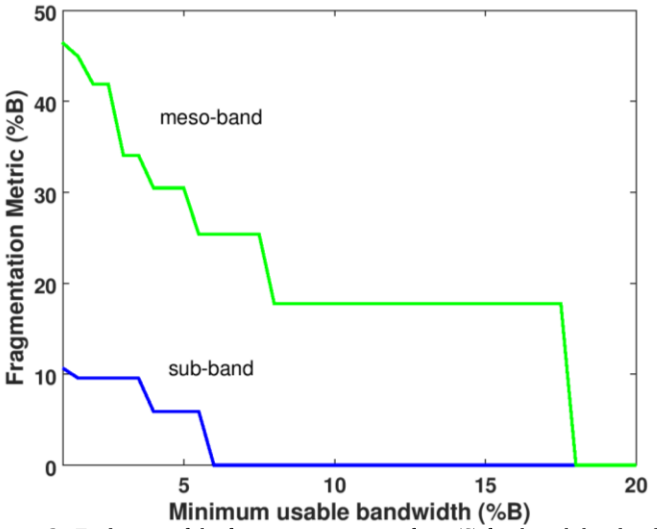

Figure 3. Evaluation of the fragmentation metric from (6) for the sub-band and meso-band MFI optimized spectrum allocations

The meso-band requirement achieves the goal of providing serviceable spectrum for other prospective users and, as demonstrated in the next section, also provides a framework for subsequent generation of physical waveforms. However, it should be noted that the trade-off in doing so is further degradation in range sidelobes. For the two examples discussed above, which are based only on theoretical spectral allocations and not actual waveform spectral content, the meso-band optimized allocation suffers a peak sidelobe level (PSL) degradation of 2.6 dB compared the sub-band optimized allocation. Thus while we may be able to realize ways in which radar spectrum can be shared, it still bears consideration whether the subsequent performance degradation is acceptable.

III. Generation of Sparse-Spectrum FM Waveforms

Now consider how the MFI-optimized meso-band sparse spectrum can be realized using physical waveforms. Here we assess three different FM waveform schemes for each meso-band, namely linear FM (LFM), first-order polyphase-coded FM (PCFM) [37], and second-order PCFM [39]. The latter two FM implementations are parameterized with underlying codes so that the combination of waveforms with different meso-bandwidths and spectral assignments comprising the overall sparse emission can be optimized in a joint manner.

The continuous phase function of the first-order PCFM structure can be expressed as [37]

$$\phi_{1\text{st}}(t) = \int_0^t \left[\sum_{n=1}^{N} \alpha_n \, g_1(\tau - (n-1)T_r) \right] d\tau + \phi_{1,0} \tag{7}$$

where α_n for $n = 1, 2, \cdots, N$ is a first-order phase-change code (analogous to instantaneous frequency), $g_1(\tau)$ is a shaping filter with time support on $[0, T_r]$ for pulsewidth $T = NT_r$, and $\phi_{1,0}$ is the initial phase. Similarly, the second-order PCFM implementation is [39]

$$\phi_{2\text{nd}}(t) = \int_0^t \int_0^\tau b_n \, g_2(\tau' - (n-1)T_r) \, d\tau' d\tau + \int_0^t \omega_{2,0} \, d\tau + \phi_{2,0} \tag{8}$$

where $\phi_{2,0}$ and $\omega_{2,0}$ are the initial phase and frequency, b_n for $n = 1, 2, \cdots, N$ is the second-order "phase-acceleration" code (analogous to instantaneous chirp rate), and $g_2(\tau')$ is the associated second-order shaping filter. The PCFM waveforms realized from these continuous phase functions are therefore

$$s_{1\text{st}}(t) = \exp\{\phi_{1\text{st}}(t)\} \tag{9}$$

and

$$s_{2\text{nd}}(t) = \exp\{\phi_{2\text{nd}}(t)\}. \tag{10}$$

As discussed in [36], the waveform time-bandwidth produce BT can be well approximated by the number of code values N. Since all of the meso-band waveforms have the same pulsewidth T, we can therefore apportion the number of code values assigned to each waveform according to the appropriate fraction of N. For example, the P = 40 meso-bands in the previous section would each be assigned a waveform parameterized by $N / P \times 50\%$ code values for optimization.

A more cohesive way to assign these code values that also provides more design flexibility is realized by first merging adjacent meso-bands into what amounts to a "macro-band", for which a single waveform can be optimized. Denoting the number of macro-bands as R, the corresponding number of code elements N_r for r = 1, 2, …, R assigned to each would depend on the bandwidth of each macro-band relative to the total bandwidth B. Additionally, each associated shaping filter has a temporal extent $T_r = T / N_r$ according to the number of code values assigned. The total radar emission is therefore the superposition

$$u_{1\text{st}}(t) = \sum_{r=1}^{R} \beta_r \, s_{1\text{st},r}(t) \tag{11}$$

or

$$u_{2\text{nd}}(t) = \sum_{r=1}^{R} \beta_r \, s_{2\text{nd},r}(t) \tag{12}$$

via (9) or (10), respectively, where the β_r terms scale the associate waveforms commensurate with their relative proportion of allocated radar bandwidth.

To illustrate these PCFM-based sparse-spectrum emissions, again consider M = 400 sub-bands, though we shall now use MFI to assign P = 29 blocks of Q = 10 sub-bands each. In this case L = 29×10 = 290, so L / M = 72.5% of the bandwidth B is allocated to the radar and the optimized

spectrum allocation in Fig. 4 is obtained. Accounting for the small spectral gap indicated in the figure, there are $R = 4$ macro-bands that can be formed (far less than what was accomplished for the 50% allocation from Fig. 2, and thus less amplitude fluctuation when combined as R distinct FM waveforms).

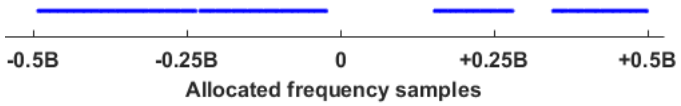

Figure 4. MFI-based sparse spectrum allocation for 72.5% usage of the total spectrum using meso-band assignment. Note the small gap near $-0.25B$.

Here the pulsewidth T is set such that $BT = 200$, which is likewise used as the value of N. For the 72.5% apportioned to the radar into the macro-bands above, we obtain the assignment $N_1 = 50$, $N_2 = 40$, $N_3 = 25$, and $N_4 = 30$, totaling 145. Based on this assignment, 4 first-order waveforms are jointly optimized according to the spectral allocation in Fig. 4 and with respect to performance metrics applied to the combined emission structure in (11). Joint optimization is likewise performed for 4 second-order waveforms via the structure of (12). The metrics used were peak sidelobe level (PSL) and integrated sidelobe level (ISL) with the optimization following the *performance diversity* paradigm outlined in [38] that involves a greedy search and alternates between these metrics to help avoid the local minima of each. In both cases a set of 4 LFM waveforms with bandwidths commensurate with the macro-band allocations above were used as initialization to optimization.

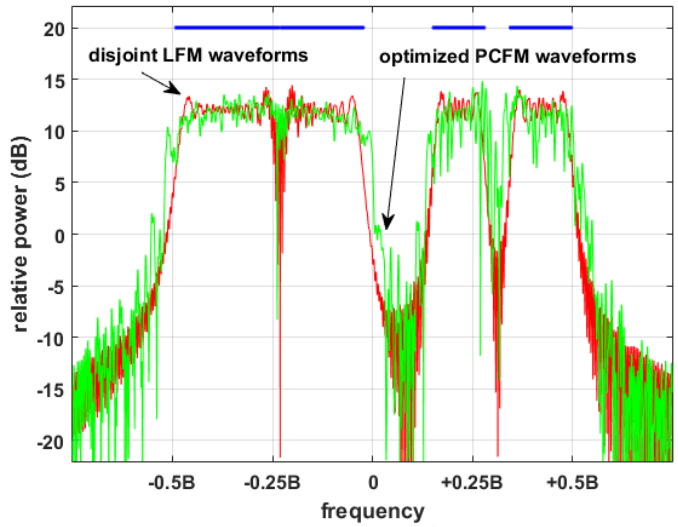

Figure 5. Sparely allocated spectral content for $R = 4$ using LFM and optimized 1st order PCFM waveform sets.

Figures 5 and 6 show the spectral content of the first-order and second-order jointly optimized emissions along with the set of 4 LFM waveforms. First of all, it is interesting to note the small spectral gap that arose from the previous MFI optimization, where, as an aside, performance was found to slightly degrade if it was filled in. To varying degrees all three waveform sets preserve this small gap. It is also found that both sets of optimized waveforms produce a modest expansion of the spectral roll-off, which is to be expected compared to the rather tight spectral containment and flat passband that is characteristic of LFM.

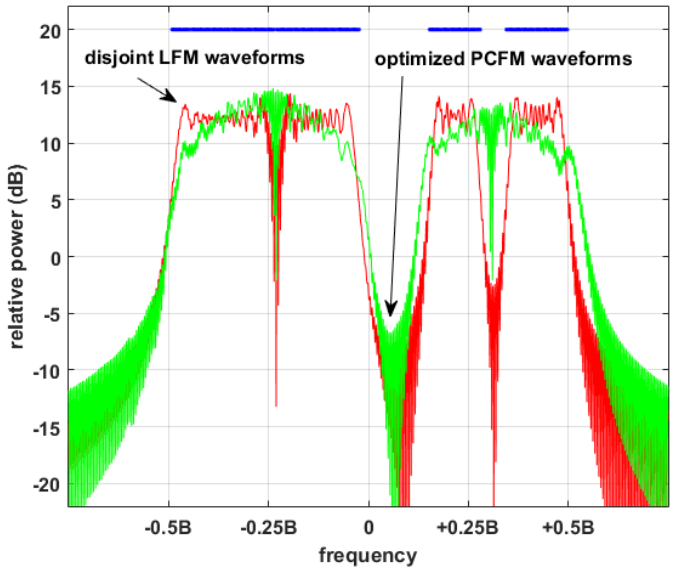

Figure 6. Sparely allocated spectral content for $R = 4$ using LFM and optimized 2nd order PCFM waveform sets

The matched filter responses for these three emissions (each a composite of $R = 4$ waveforms) are depicted in Figs. 7-9. The cases involving disjoint LFM and the optimized first-order emission realize some shoulder lobes near the mainlobe that are not present for the second-order emission. However, the latter also has far-out sidelobes that are higher than the other two cases. The near-in shoulder lobes notwithstanding, one could make the argument that the optimized first-order emission is the best of these for this particular scenario since it produces a sidelobe response that is relatively flat. Of course, different sparse spectrum allocations could produce different optimized emission structures. The point of this demonstration is that actual physical waveforms can be obtained that may achieve the sidelobe requirements for operational radar.

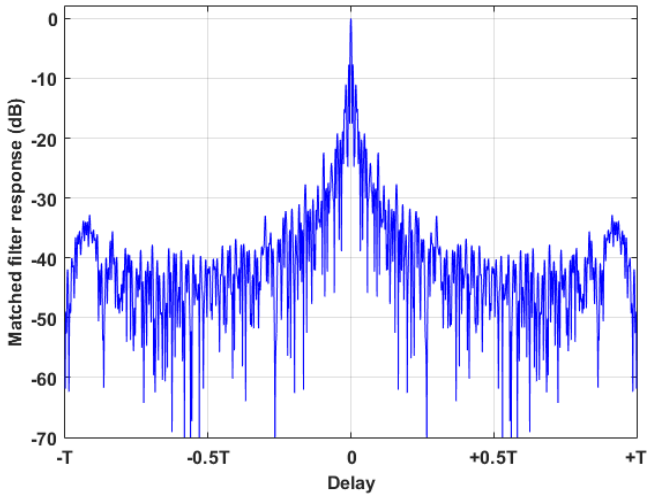

Figure 7. Matched filter responses for the composite emissions formed from a set of $R = 4$ disjoint LFM waveforms

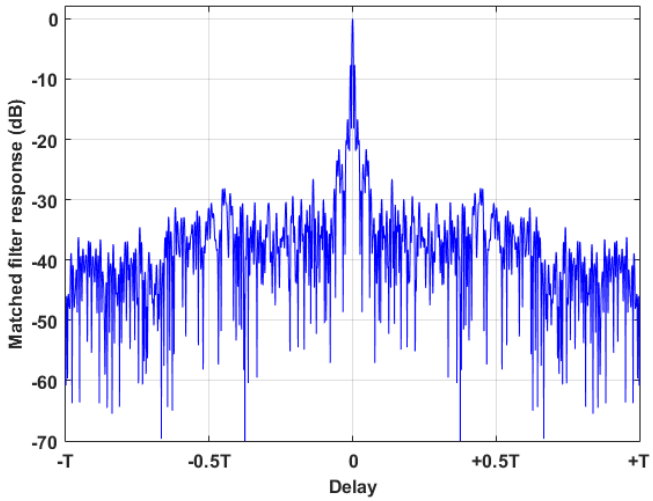

Figure 8. Matched filter responses for the composite emissions formed from a set of $R = 4$ optimized 1st order PCFM waveforms

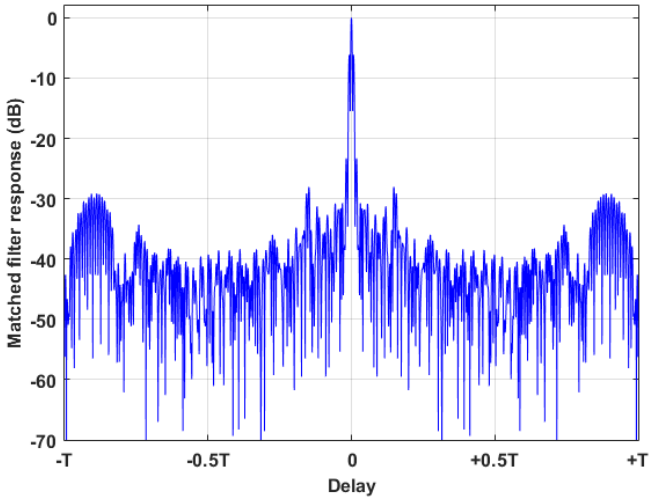

Figure 9. Matched filter responses for the composite emissions formed from a set of $R = 4$ optimized 2nd order PCFM waveforms

IV. CONCLUSIONS

Given a maximum percent occupancy the marginal Fisher's information (MFI) optimization of sparse radar spectrum has been considered from the perspective of ensuring sufficient serviceable spectral regions for other users to occupy. Without such a requirement, sparse spectrum optimization tends to spread more evenly across the total bandwidth, being driven by an imperative only to optimize radar performance (i.e. make the best out of the spectrum loss). By reducing the spectral fragmentation, however, the radar performance is necessarily degraded even further than what is incurred by the loss in spectrum alone.

It was then demonstrated that sets of FM waveforms could be realized and even optimized within this MFI-generated sparse spectrum arrangement. Individually, these physical waveforms can be readily generated by a radar transmitter, though their combination produces a non-zero peak-to-average power ratio (PAPR) [44] that is rather difficult to emit at high power. More complex transmitter architectures [45], predistortion [46,47], or hardware-in-the-loop waveform optimization [48-50] could potentially be used to address this limitation, though these also come with their own performance trade-offs and limitations.

REFERENCES

[1] M. Lauridsen, L.C. Gimenez, I. Rodriguez, T.B. Sorensen, P. Mogensen, "From LTE to 5G for connected mobility," *IEEE Comm. Mag.*, vol. 55, no. 2, pp. 156-162, Mar 2017.

[2] Y. Daldoul, D. Meddour, A. Ksentini, "IEEE 802.11ac: effect of channel bonding on spectrum utilization in dense environments," *IEEE Intl. Conf. Comm.*, Paris, France, May 2017.

[3] F. Lv, H. Zhu, H. Xue, Y. Zhu, S. Chang, M. Dong, M. Li, "An empirical study on urban IEEE 802.11p vehicle-to-vehicle communication," *IEEE Intl. Conf. Sensing, Communication, and Networking*, London, UK, June 2016.

[4] H. Griffiths, L. Cohen, S. Watts, E. Mokole, C. Baker, M. Wicks, S. Blunt, "Radar spectrum engineering and management: technical and regulatory issues," *Proc. IEEE*, vol. 103, no. 1, pp. 85-102, Jan. 2015.

[5] S.D. Blunt, P. Yatham, "Waveform design for radar-embedded communication," *Intl. Waveform Diversity & Design Conf.*, Pisa, Italy, June 2007.

[6] W. Liu, Y. Lu, M. Lesturgie, "Optimal sparse waveform design for HFSWR system," *Intl. Waveform Diversity & Design Conf.*, Pisa, Italy, June 2007.

[7] I.W. Selesnick, S.U. Pillai, R. Zheng "An iterative algorithm for the construction of notched chirp signals," *IEEE Intl. Radar Conf.*, Arlington, VA, USA, May 2010.

[8] M.R. Cook, T. Higgins, A.K. Shackelford, "Thinned spectrum radar waveforms," *Intl. Waveform Diversity & Design Conf.*, Niagara Falls, ON, Canada, Aug. 2010.

[9] K. Gerlach, M.R. Frey, M.J. Steiner, A. Shackelford, "Spectral nulling on transmit via nonlinear FM radar waveforms," *IEEE Trans. Aerospace & Electronic Systems*, vol. 47, no. 2, pp. 1507-1515, Apr. 2011.

[10] I.W. Selesnick, S.U. Pillai, "Chirp-like transmit waveforms with multiple frequency-notches," *IEEE Radar Conf.*, Kansas City, MO, USA, May 2011.

[11] Y. Nijsure, Y. Chen, C. Yuen, Y. H. Chew, "Location-aware spectrum and power allocation in joint cognitive communication-radar networks," *6th CROWNCOM Conf.*, Osaka, Japan, June 2011.

[12] R. Saruthirathanaworakun, J. Peha, L. Correia, "Opportunistic sharing between rotating radar and cellular," *IEEE J. Selected Areas Communications*, vol. 30, no. 10, pp.1900-1910, Nov. 2012.

[13] M. Tercero, K. Sung, J. Zander, "Exploiting temporal secondary access opportunities in radar spectrum", *Wireless Personal Communications*, vol 72, no. 3, pp 1663–1674, Oct. 2013.

[14] A. Turlapaty, Y. Jin, "A joint design of transmit waveforms for radar and communications systems in coexistence", *IEEE Radar Conf.*, Cincinnati, OH, USA, May 2014.

[15] C. Shahriar, A. Abdelhadi, T.C. Clancy, "Overlapped-MIMO radar waveform design for coexistence with communication systems," *IEEE Intl. Comm. & Networking Conf.*, New Orleans, LA, USA, Mar. 2015.

[16] J.G. Metcalf, C. Sahin, S.D. Blunt, M. Rangaswamy, "Analysis of symbol design strategies for intrapulse radar-embedded communications," *IEEE Trans. Aerospace & Electronic Systems*, vol. 51, no. 4, pp. 2914-2931, Oct. 2015.

[17] J. Jakabosky, S.D. Blunt, A. Martone, "Incorporating hopped spectral gaps into nonrecurrent nonlinear FMCW radar emissions," *IEEE CAMSAP Workshop*, Cancun, Mexico, Dec. 2015.

[18] B. Li, H. Kumar, A. Petropulu, "A joint design approach for spectrum sharing between radar and communication systems," *IEEE ICASSP Conf.*, Shanghai, China, May 2016.

[19] E.H.G. Yousif, M.C. Filippou, F. Khan, T. Ratnarajah, M. Sellathurai, "A new LSA-based approach for spectral coexistence of MIMO radar and wireless communications systems," *IEEE Intl. Conf. Comm.*, Kuala Lumpur, Malaysia, May 2016.

[20] P.S. Tan, J.M. Stiles, S.D. Blunt, "Optimizing sparse allocation for radar spectrum sharing," *IEEE Radar Conf*., Philadelphia, PA, USA, May 2016.

[21] J. Jakabosky, B. Ravenscroft, S.D. Blunt, A. Martone, "Gapped spectrum shaping for tandem-hopped radar/communications & cognitive sensing," *IEEE Radar Conf*., Philadelphia, PA, USA, May 2016.

[22] M. La Manna, M. La Manna, "Cognitive radar waveforms for frequency dense environments", *IEEE Radar Conf*., Seattle, WA, USA May 2017.

[23] B. Ravenscroft, P.M. McCormick, S.D. Blunt, J. Jakabosky, J.G. Metcalf, "Tandem-hopped OFDM communications in spectral gaps of FM noise radar," *IEEE Radar Conf*., Seattle, WA, May 2017.

[24] C. Sahin, J. Jakabosky, P. McCormick, J. Metcalf, S. Blunt, "A novel approach for embedding communication symbols into physical radar waveforms," *IEEE Radar Conf.*, Seattle, WA, May 2017.

[25] P.M. McCormick, S.D. Blunt, J. Metcalf, "Simultaneous radar and communication emissions from a common aperture, part I: theory," *IEEE Radar Conf*., Seattle, WA, May 2017.

[26] P.M. McCormick, A. Duly, B. Ravenscroft, S.D. Blunt, J. Metcalf, "Simultaneous radar and communication emissions from a common aperture, part II: experimentation," *IEEE Radar Conf*., Seattle, WA, May 2017.

[27] H. Wang, J. Johnson, C. Baker, "Spectrum sharing between communications and ATC radar systems", *IET Radar, Sonar & Navigation*, vol. 11, no. 6, pp. 994-1001, July 2017.

[28] B. Ravenscroft, P.M. McCormick, S.D. Blunt, E. Perrins, J.G. Metcalf, "A power-efficient formulation of tandem-hopped radar & communications," submitted to *IEEE Radar Conf.*, Oklahoma City, OK, Apr. 2018.

[29] J.W. Owen, B. Ravenscroft, B.H. Kirk, S.D. Blunt, C.T. Allen, A.F. Martone, K.D. Sherbondy, R.M. Narayanan, "Experimental demonstration of cognitive spectrum sensing & notching for radar," submitted to *IEEE Radar Conf.*, Oklahoma City, OK, Apr. 2018.

[30] S.D. Blunt and E.S. Perrins, eds., *Radar & Communication Spectrum Sharing*, IET, 2018.

[31] J.D. Jenshak, J.M. Stiles, "A fast method for designing optimal transmit codes for radar," *IEEE Radar Conf*., Rome, Italy, May 2008.

[32] J. Stiles, J. Jenshak, "Sparse array construction using marginal Fisher's information," *Intl. Waveform Diversity & Design Conf.*, Orlando, FL, USA, Feb. 2009.

[33] J. Jenshak, J. Stiles, "Computation of QAM radar transmit signals with low autocorellation sidelobes," *IEEE Radar Conf.*, Pasadena, CA, USA, May 2009.

[34] J. Jakabosky, P. Anglin, M.R. Cook, S.D. Blunt, J. Stiles, "Non-linear FM waveform design using marginal Fisher's information with the CPM framework," *IEEE Radar Conf.*, Kansas City, MO, USA, May 2011.

[35] A.T. Moffet, "Minimum-redundancy linear arrays," *IEEE Trans. Antennas & Propagation*, vol. 16, no. 2, pp. 172-175, Mar 1968.

[36] A. Martone, K. Ranney, K. Sherbondy, K. Gallagher, S. Blunt, "Spectrum allocation for non-cooperative radar coexistence," *IEEE Trans. Aerospace & Electronic Systems*, vol. 54, no. 1, pp. 90-105, Feb. 2018.

[37] S.D. Blunt, M. Cook, J. Jakabosky, J. de Graaf, and E. Perrins, "Polyphase-coded FM (PCFM) radar waveforms, part I: implementation," *IEEE Trans. Aerospace & Electronic Systems*, vol. 50, no. 3, pp. 2218-2229, July 2014.

[38] S.D. Blunt, J. Jakabosky, M. Cook, J. Stiles, S. Seguin, E.L. Mokole, "Polyphase-coded FM (PCFM) radar waveforms, part II: optimization," *IEEE Trans. Aerospace & Electronic Systems*, vol. 50, no. 3, pp. 2230-2241, July 2014.

[39] P.S. Tan, J. Jakabosky, J. M. Stiles, S.D. Blunt, "On higher-order representations of polyphase-coded FM radar waveforms," *IEEE Intl. Radar Conf*., Arlington, VA, USA, May 2015.

[40] S.M. Kay, *Fundamentals of Statistical Signal Processing: Estimation Theory*, Prentice Hall, 1993.

[41] H.V. Trees, *Detection, Estimation, and Modulation Theory*, vol. 1, John Riley & Sons, 2001.

[42] V.V. Fedorov, *Theory of Optimal Experiments*, Elsevier, 1972.

[43] S.D. Blunt, E.L. Mokole, "An overview of radar waveform diversity," *IEEE AESS Systems Magazine*, vol. 31, no. 11, pp. 2-42, Nov. 2016.

[44] E. Costa, M. Midrio, and S. Pupolin, "Impact of amplifier nonlinearities on OFDM transmission system performance," *IEEE Communications Letters*, vol. 3, no. 2, pp. 37-39, Feb. 1999.

[45] F.H. Raab, P. Asbeck, S. Cripps, P.B. Kenington, Z.B. Popovic, N. Pothecary, J.F. Sevic, and N.O. Sokal, "Power amplifiers and transmitters for RF and microwave," *IEEE Trans. Microwave Theory & Techniques*, vol. 50, no. 3, pp. 814-826, Mar. 2002.

[46] F.M. Ghannouchi and O. Hammi, "Behavioral modeling and predistortion," *IEEE Microwave Magazine*, pp. 52-64, Dec. 2009.

[47] Z. Dunn, M. Yeary, C. Fulton, R. Rincon, "Impedance-dependent wideband digital predistortion of solid-state radar amplifiers," *IEEE Trans. Aerospace & Electronic Systems*, vol. 53, no. 5, pp. 2290-2303, Oct. 2017.

[48] J. Jakabosky, L. Ryan, and S.D. Blunt, "Transmitter-in-the-loop optimization of distorted OFDM radar emissions," *IEEE Radar Conf.* Ottawa, Canada, Apr./May 2013.

[49] L. Ryan, J. Jakabosky, S.D. Blunt, C. Allen, and L. Cohen, "Optimizing polyphase-coded FM waveforms within a LINC transmit architecture," *IEEE Radar Conf*., Cincinnati, OH, May 2014.

[50] D. Eustice, C. Latham, C. Baylis, R.J. Marks, L. Cohen, "Amplifier-in-the-loop adaptive radar waveform synthesis," *IEEE Trans. Aerospace & Electronic Systems*, vol. 53, no. 2, pp. 826-836, Apr. 2017.